Int. J. Electrochem. Sci., 13 **(2018)** 9505 – 9519, doi: 10.20964/2018.10.07

International Journal of
ELECTROCHEMICAL
SCIENCE
www.electrochemsci.org

Effects of Spangle Size on Performances of Hot-dip 55%Al-Zn Alloy Coating

Taixiong Guo[1,2,*], *Changsheng Liu*[1], *Changrong Ran*[2], *Xueqiang Dong*[2]

[1] School of Materials Science and Engineering, Northeastern University, Shengyang 110819, Liaoning, China
[2] Pangang Group Research Institute Co. Ltd., Panzhihua 617000, Sichuan, China
[*]E-mail: guotaixiong@126.com

Received: 7 April 2018 / *Accepted:* 7 June 2018 / *Published:* 1 September 2018

The influences of spangle on corrosion resistance, formability and paintability of hot-dip 55%Al-Zn alloy coating (GL) steel sheet are the main concern for household appliance manufacturers. In this study, the effects of spangle size on those performances of GL steel sheet were investigated through electrochemistry, neutral salt spray, bending and Erichsen cupping, and electrostatic powder spraying tests. The microstructure and surface morphology of the samples were analyzed by scanning electron microscopy (SEM), atomic force microscopy (AFM), nano indentation, surface roughometer and glossmeter. The influencing mechanisms of spangle size were also discussed. The results showed that decreasing the spangle size refined Al-rich dendrites, reduced dendrite spacing, and segregated Zn-rich phase. This, in turn, improved both the corrosion resistance and formability of the coatings. The electrostatic powder spraying tests confirmed the good paintability of all samples with different spangle sizes.

Keywords: 55%Al-Zn alloy coating; Spangle size; Corrosion resistance; Formability; Paintability

1. INTRODUCTION

Zinc and zinc alloy coatings are two common methods used to prevent the corrosion of steel sheets in atmospheric environment. The most widely used technologies in industrial production are hot-dip pure zinc (hereinafter referred to as GI) and 55%Al-43.4%Zn-1.6%Si alloy coating (hereinafter referred to as GL) steel sheets. The GL steel sheet was developed by Bethlehem Steel Co. in the 1970s. Due to its excellent corrosion resistance, decorative performance, and high-temperature oxidation resistance, GL steel sheet has been widely used in various fields, such as building, transportation, and electrical manufacturing. Meanwhile, with the development of hot-dip technology and improvement of

GL quality, the applications of GL steel sheets in household appliance manufacturing, e.g., air conditioners, refrigerators, and washing machines, showed a gradual increase. Consistent with GI containing Pb, Sb or Bi, spangle became a distinguishing characteristic of GL steel sheet. Previous studies found that spangle significantly affects the performances of GI steel sheets [1-5]. Therefore, promotion and application of GL steel sheets in household appliance manufacturing should specify the effects of the spangle size on coating properties.

Research and applications addressing GI have started more than 100 years before those of using GL, leading to a much less comprehensive study of the characteristics of GL compared to GI steel sheets. Previous studies on GL steel sheets mainly focused on the formation and microstructure of coatings [6-17], as well as the corrosion behaviors and mechanisms under various environments [18-28]. In addition, Willem et al. studied the effects of several processing parameters, such as degrease cleaning, furnace atmosphere, and Si content on spangle size [29-32]. In recent years, the growth of GL steel sheet applications focused more attention on issues of spangle size. To obtain mini-spangle meeting household appliance users expectations, Peng et al. studied the effects of Si content and addition of Ti, Mg, B and REs (La, Ce) on the refinement of α-Al dendrite (determines spangle size) [33-36]. However, the influences of spangle size on coating properties are still not reported. Corrosion resistance, formability, and paintability are the main performance requirements of coated steel sheets concerning household appliance users. Therefore, in this study, a series of tests and analyses were conducted to investigate the effects of spangle size on those performances of GL steel sheets.

2. EXPERIMENTAL

The test materials were obtained from an industrial hot-dip Al-Zn production line. The grade of the experimental steel was DX51D+AZ, with steel substrate thickness of 1.0 mm, coating weight of 150 g/m^2, and spangle size of 0.5-4.0 mm. The spangle size was defined as the average diameter of spangles, which was determined by using the intersection method established in the ASTM E 112 standard [1].

For coated steel sheets, the corrosion resistance should be the primary concern for users. Electrochemical testing is one of the most common methods for analyzing material corrosion. Furthermore, neutral salt spray test (NSST) was often employed by household appliance manufacturers to evaluate the coating corrosion resistance. Therefore, both of them were utilized here to evaluate the coatings corrosion resistance. A CHI650A electrochemical workstation with three-electrode system was employed for electrochemical tests, with 213-type Pt used as auxiliary electrode and 217-type saturated calomel as reference electrode (SCE). The test solution contained 3.5% NaCl solution prepared with de-ionized water. The testing area was maintained at 1 cm^2 by sealing the rest of the specimen with tape. Potentiodynamic polarization curves were measured between -0.5 V to -1.5 V (vs SCE) at a scan rate of 5 mV/s. Electrochemical impedance spectroscopy (EIS) were measured at the frequency range of 100 kHz - 10 mHz with an AC amplitude of 10 mV. The NSST was conducted according to the China National Standard GB/T 10125. The corrosive medium was made of NaCl

solution at concentration of 50 ± 5 g/L. The experimental results were evaluated based on the formation time of red rust.

The cracking extents of the coatings after bending and cupping deformation, as well as NSST results of specimens with different spangle sizes were used to evaluate the coating formability. The bending tests were conducted according to Standard GB/T 13448. The angle of bending was set to 180° and bend diameter was 0 (0 T bending deformation). The Erichsen cupping test was conducted according to Standard GB/T 4156, which stopped at stamping depth of 7 mm. After completion of testing, the specimens were taken out to observe the cracking extent or placed into a salt spray chamber for NSST. To evaluate the cracking extent, both crack density and crack width were comprehensively considered. For the NSST, the formation time of red rust within the deformed region was used as an evaluation index.

The coating paintability was evaluated by surface roughness, glossiness, and adhesion of specimens with different spangle sizes after electrostatic powder spraying. The electrostatic powder spraying tests were conducted in an air conditioning production line provided by one household appliance company. Commonly used polyurethane paint was employed, and thickness was set to about 30 μm. The adhesion of painting layer was evaluated by cross-cut test, conducted according to Standard GB/T 9286.

The microstructure and surface morphologies of specimens were analyzed by JSM-5600LV scanning electron microscopy (SEM), atomic force microscopy (AFM), nano indention, Mitutoyo SJ-410 surface roughometer, and BYK4563 glossmeter.

3. RESULTS AND DISCUSSION

3.1 Effect of spangle size on corrosion resistance

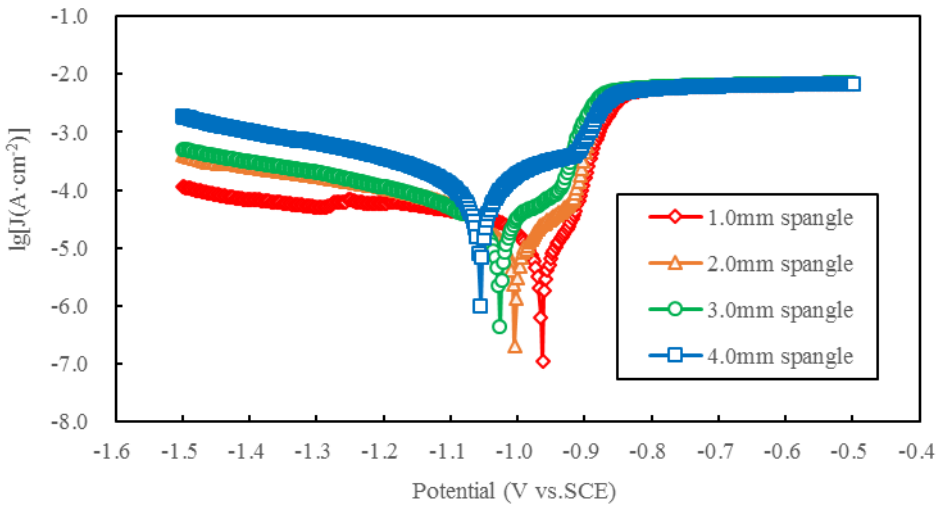

Figure 1. Potentiodynamic polarization curves of specimens with different spangle sizes in 3.5% NaCl solution, at a scan rate of 5 mV/s.

Figure 1 shows the potentiodynamic polarization curves of specimens with different spangle sizes, and the fitting data of the electrochemical parameters are listed in Table 1. As spangle size decreased, the corrosion potential shifted towards positive values, and corrosion current declined. These changes indicated that the obstruction against chloride ion (corrosive medium) in solution became stronger for coatings deposited on specimens with mini spangles. This raised the charge transfer resistance of the system and reduced the electron transfer rate between the anode and cathode, slowing down both the oxidation reaction at the anode and the reduction reaction of the cathode. The active dissolution rate of the coating declined and the protective effect of the coating on steel substrate lasted longer.

Table 1. Fitting data of electrochemical parameters of specimens with different spangle sizes in 3.5% NaCl solution -evaluated via potentiodynamic polarization measurement.

Spangle size (mm)	Corrosion potential (E_{corr}, V)	Corrosion current density (J_{corr}, A/cm^2)	Polarization resistance (R_p, Ω•cm^2)
1.0	-0.959	5.35×10^{-6}	2632
2.0	-1.000	7.38×10^{-6}	2320
3.0	-1.029	9.17×10^{-6}	1308
4.0	-1.061	6.57×10^{-5}	460

Figure 2 depicts the EIS Nyquist plots of the specimens. The Nyquist plots of the specimens with different spangle sizes showed similar shapes (semicircles), indicating the characteristic of a capacitive impedance loop without diffusion impedance. This suggested that the corrosion process should be electrochemically-controlled. With decreased spangle size, the impedance loop significantly enlarged, indicating higher corrosion resistance, lower corrosion rate, and improved corrosion resistance. These data were consistent with the potential dynamic polarization test results.

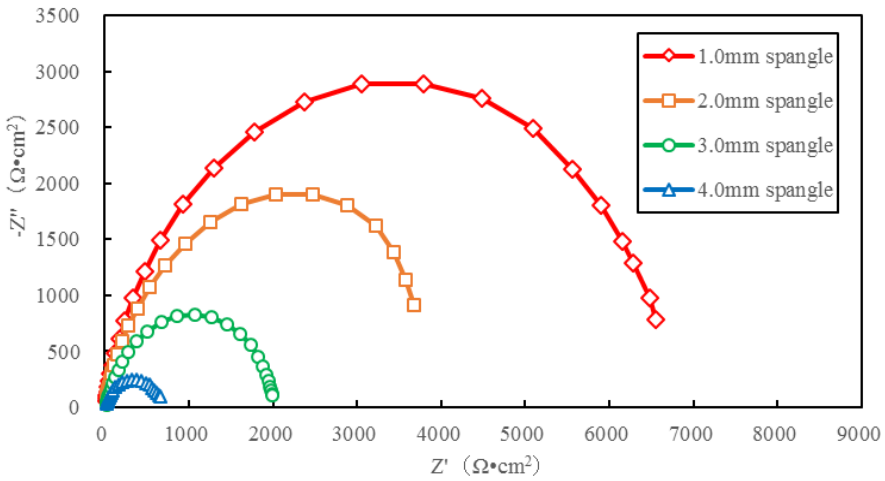

Figure 2. Nyquist plots of specimens with different spangle sizes in 3.5% NaCl solution, at the frequency range of 100 kHz-10 mHz with an AC amplitude of 10 mV.

NSST results of the specimens with different spangle sizes are shown in Figure 3. The decrease in spangle size extended the formation time of red rust. This suggests that corrosion resistance of specimens with mini spangles were better than those of specimens with large spangles. This agreed well with the electrochemical test results. In addition, NSST results demonstrated great differences in formation time of red rust even under the same conditions of coating weight and spangle size. This could be issued from the characteristic of neutral salt spray tests, hence several parallel tests were required to reach better conclusions.

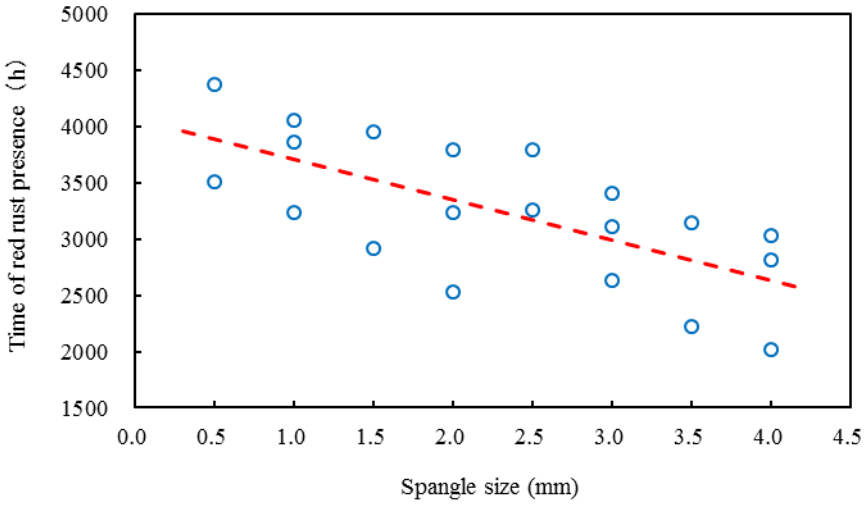

Figure 3. Relationship between spangle size and formation time of red rust in NSST with 50 ± 5g/L NaCl solution.

As mentioned above, the electrochemical and NSST results indicated that smaller spangle was beneficial for improved coating corrosion resistance. These should be determined by the coating micro-structural characteristics and corrosion mechanism.

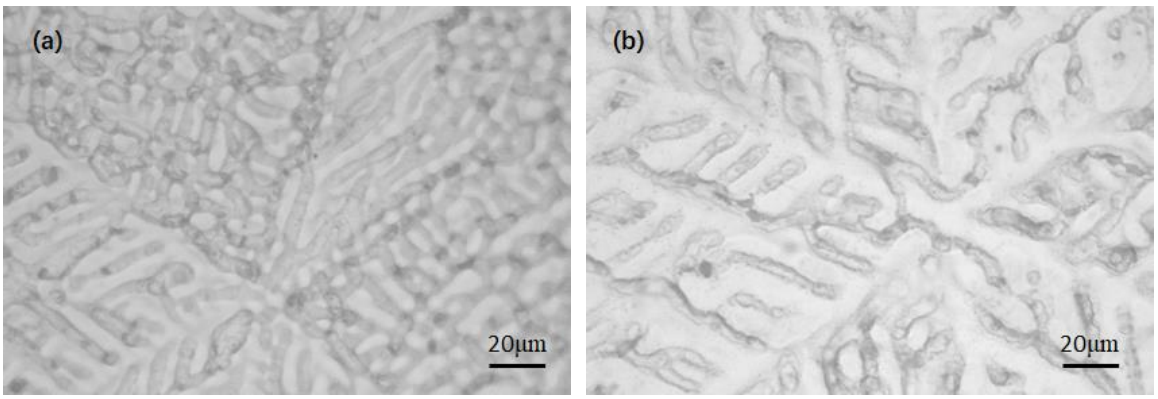

Figure 4. Surface micro-morphology of specimens with (a) mini spangle and (b) large spangle.

Previous studies [12, 13, 20, 37] showed that the inner layer of GL coating was made of Fe-Al-Zn-Si intermetallic compounds (IMC) while the overlay consisted of Al-rich phase (α-Al), Zn-rich phase (β-Zn), and needle Si-rich phase. The composition of Al-rich phase consisted of 64.5%Al+35.3%Zn+0.2%Si, with a volume fraction of ~80%. The composition of Zn-rich phase contained 20.4%Al+78.9%Zn+0.7%Si, with a volume fraction of ~20%. The micro-morphology (SEM image) of specimens are shown in Figures 4 and 5. In comparison to specimens with large spangles, the coatings on specimens with mini spangles revealed finer Al-rich dendrites and smaller secondary dendritic spacing (finer Zn-rich phase). The Al-rich phase was divided into smaller islands by the Zn-rich phase. The amount of Zn-rich phase that could penetrate through Al-rich phase from top surface to the intermetallic layer reduced to yield more obvious network structure of the coating and small grid.

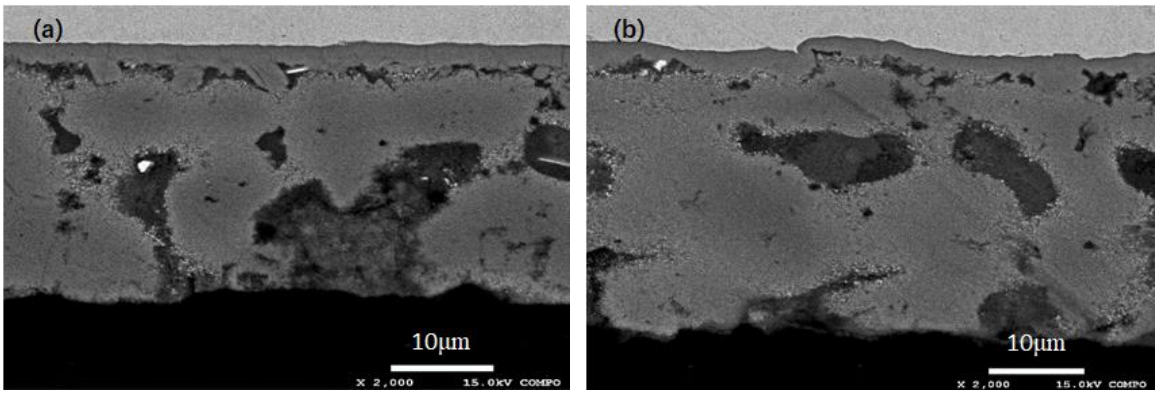

Figure 5. Micro-morphology of cross-section coating with (a) mini spangle and (b) large spangle.

In a corrosive environment [18, 24, 27], preferential corrosion would occur within Zn-rich phase on the coating surface to yield $Zn_5(CO_3)_2(OH)_6$ as the main corrosion product. In time, the corrosion of Zn-rich phase should penetrate into the coating along the region between dendrites. Furthermore, the corrosion of Al-rich dendrites would begin to occur to change the main corrosion product into $Zn_6Al_2(OH)_{16}CO_3{\bullet}nH_2O$. Compared to $Zn_6(OH)_8Cl_2{\bullet}H_2O$ as main corrosion product of GI coating, $Zn_6Al_2(OH)_{16}CO_3{\bullet}nH_2O$ appeared denser and uniform with better resistance against penetration of corrosive medium. Hence, it can slow the corrosion expansion.

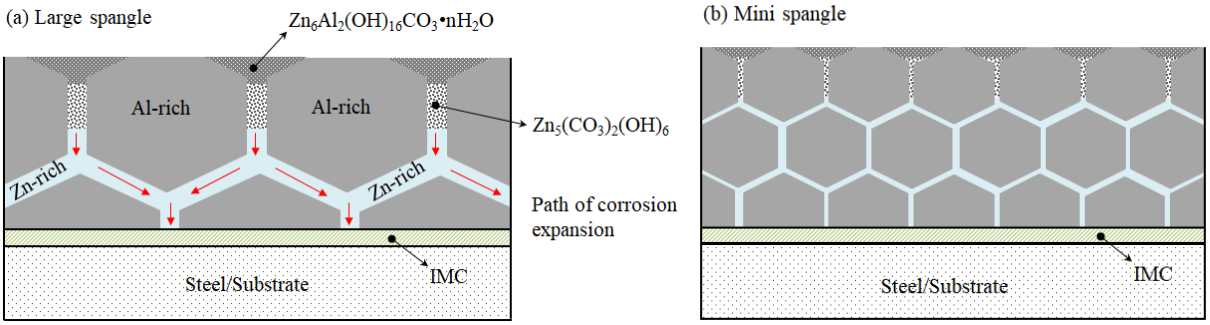

Figure 6. Schematic representation of corrosion expansion in the coating.

In summary, the reduced spangle size refined Zn-rich and Al-rich phases, narrowing corrosion expansion paths in the coating and increased curvature. In addition, the filling of dense corrosion product blocked corrosion expansion within the coating and improved the corrosion resistance. The schematic representation is illustrated in Figure 6. Selverian et al. [13, 14, 33-34] also found a decrease in Si content in bath, Ti addition or increase in cooling rate after plating should increase the nucleation rate of Al-rich dendrite or inhibit growth rate. Hence, spangle size and Al-rich dendrite arm spacing decreased. Moreira et al. [20, 35] suggested that a refined network consisting of Zn-rich and Al-rich phases can preserve corrosion products, which would thus be beneficial to prevent local penetrating corrosion. These results show that the corrosion resistance increases with the decrease of spangle size, which is consistent with the results obtained in the present experiment. In addition, the corrosion resistance of GI with small spangle was also better than that of large spangle. However, the influencing mechanism differed. The main reasons of the deterioration of corrosion resistance for GI with large spangles can be found in two aspects: First, addition of Pb, Sb, or Bi would be segregated at grain boundaries and allow the formation of small corrosion cells [38-40]. Second, (00.2) basal plane texture components would be weakened, thus decreasing corrosion resistances of the coating [4, 5].

3.2 Effect of spangle size on formability

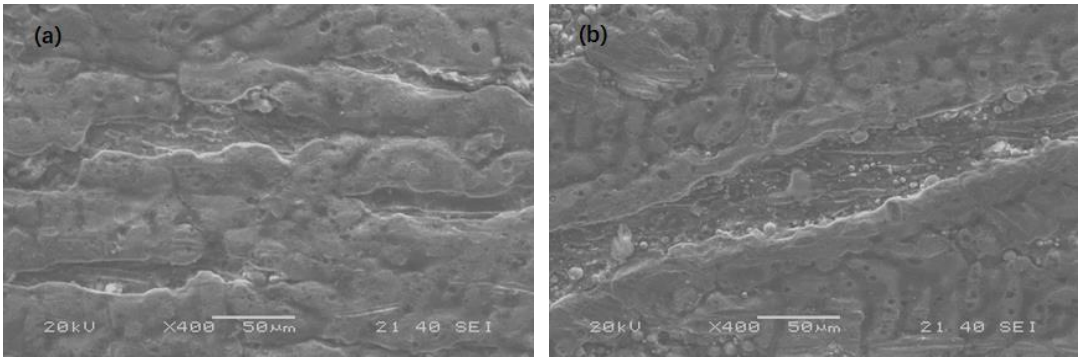

Figure 7. Surface micro-morphology of 0 T bending deformed specimens with (a) mini spangle and (b) large spangle.

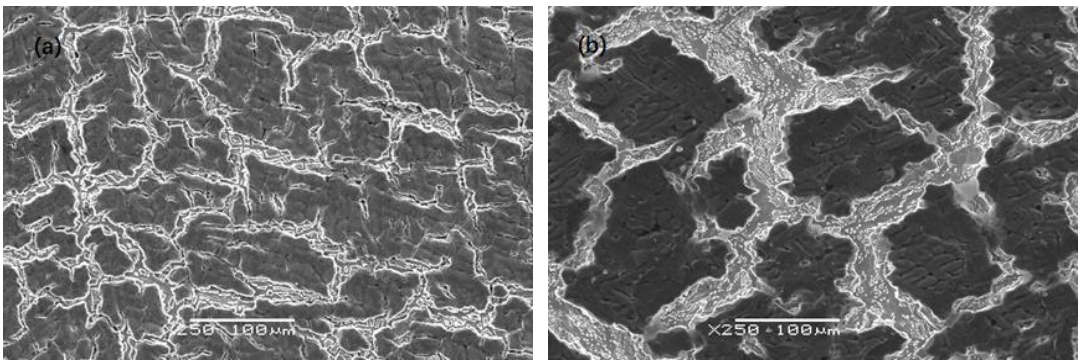

Figure 8. Surface micro-morphology of Erichsen cupping deformed specimens (stamping depth of 7 mm) with (a) mini spangle and (b) large spangle.

The surface micro-morphology (SEM image) of deformed specimens is shown in Figures 7 and 8. After bending and Erichsen cupping deformation, different extent of cracks occurred within coating deformation regions. The cracks in bending deformed specimens were strip-like while those in cupping deformed specimen were interlaced forming networks. Compared to cupping deformed specimen, the cracks in bent specimen coating were relatively sparser. However, the cracks were longer and wider, with larger amounts of cracks penetrating the steel substrate. Compared to specimens with large spangles, the cracks of the specimens with mini spangles were denser, shorter and narrower, while the amounts of cracks penetrating the steel substrate were lower.

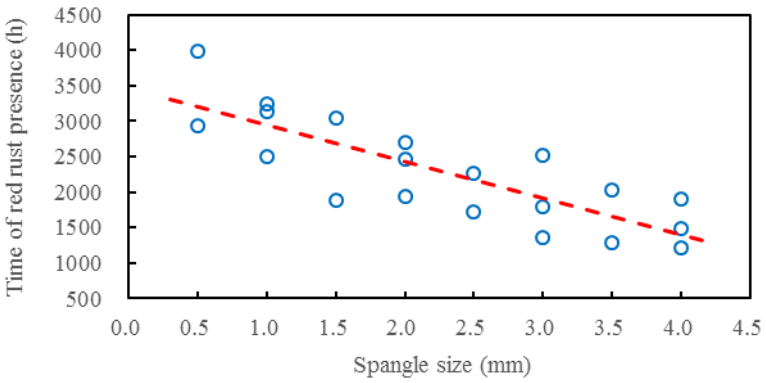

Figure 9. Relationship between spangle size and formation time of red rust in NSST with 50 ± 5 g/L NaCl solution after 0 T bending deformation.

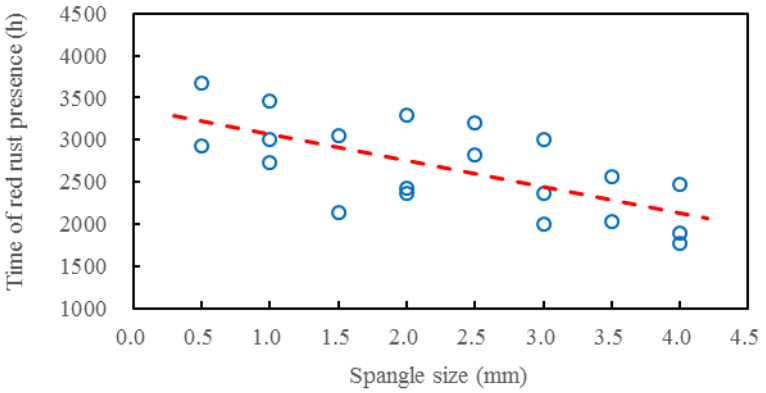

Figure 10. Relationship between spangle size and formation time of red rust in NSST with 50 ± 5 g/L NaCl solution after Erichsen cupping deformation (stamping depth of 7 mm).

The relationship between the time of red rust present in NSST after deformation and spangle size are illustrated in Figures 9 and 10. For bending and cupping deformed specimens, the formation time of red rust tended to increase as spangle size decreased. Figures 9 and 10 estimated the formation time of red rust in NSST of bending deformed specimen to approximately 1500-3000 h, and that of cupping deformed specimen was about 2000-3500 h. The corresponding formation time of non-deformed specimen was 2500-4000 h (Figure 3). In other words, the corrosion resistance of deformed

specimens decreased and the corrosion resistance of bending deformed sample weakened when compared to that of cupping deformed sample. This indicated that the formation time of red rust on deformed specimens in NSST may indirectly reflect the coating formability. In general, the coating formability of specimen with mini spangles should be better than that of large spangles.

The coating formability could also be determined by its microstructure. The main factors affect the coating ductility should be phase components (or composition), crystal structure, grain size, crystallographic orientation, and coating thickness [37, 41].

Ramamurty et al. [42, 43] suggested that the plasticity of metallic material could be reflected by its hardness to some extent. Hardness tests had been widely used to evaluate the mechanical properties of materials. The indentation hardness test was typically used to study the elastic-plastic behavior of materials, which was helpful to obtain insights into the microscopic mechanisms of plastic deformation. The hardness experiments of steel substrate, Al-rich, Zn-rich and Si-rich phases at the cross-section of GL sheet were carried out via nano indenter and the results are shown in Figure 11. The Si-rich phase was the hardest and Zn-rich phase was the softest. The hardness of the Al-rich phase was located between values of steel substrate and Zn-rich phase. In general, greater hardness induces higher strength but lower plasticity. Due to differences in plasticity of the phases consisting of GL coating, incompatible deformation tended to occur during the deformation process, leading to coating crack. Furthermore, the data demonstrated that the cracks would be originated from the hard-brittle Si-rich phase in the process of deformation.

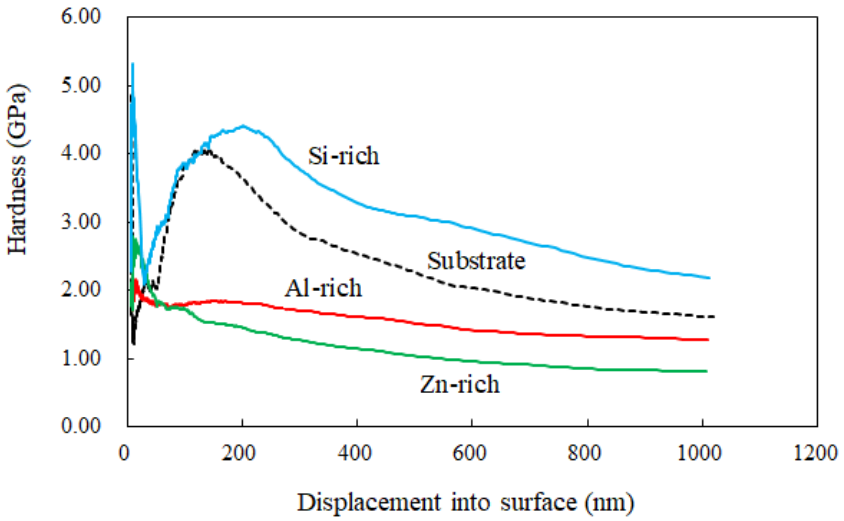

Figure 11. Nano indentation hardness of various phases in the coating.

In term of crystal structure [12, 44], the Al-rich phase is face-centered cubic (fcc), the zinc-rich phase is hexagonal close-packed (hcp), and the steel substrate is body-centered cubic (bcc). Metals with fcc or bcc lattice structures have more slip systems, and better deformation coordination, and hence good plasticity [45]. That is, the zinc-rich phase holds a reduced number of available slip systems compared to the Al-rich phase, making plastic deformation more difficult. Furthermore, the Si-rich phase, which is the source of cracking, is located in the zinc-rich phase. Therefore, with

increased deformation, the crack would propagate along the zinc-rich phase. Willis et al. also found that cracks in GL coating originated from hard-brittle Si-rich phase, intermetallic layer or slag particles, and cracks expanded along Zn-rich phase [44]. This is similar to the grain-boundary cracking that occurs during the deformation of GI coating [46]. The zinc-rich phase of GL coating and grain boundary of GI coating are both weak regions for plastic deformation.

According to the cracking mechanism of GL coating deformation, as mentioned above, reduction in spangle size fined network structure in coating (Figures 4, 5, and 6), dispersing crack source, and increased crack interaction. After deformation, the cracks densified, shorten, and narrowed (Figures 7 and 8). Furthermore, the compatibility of deformation between phases in the coating would be improved and the amounts of cracks penetrating the steel substrate reduced. In addition, due to different deformation mode and strain condition, the morphology of cracks differed. In fact, grain refinement is beneficial to increase strength and improve plasticity [47, 48]. Park et al. have also reported that the spangle size of GL increased with Pb addition, and the bending deformation performance deteriorated [49]. However, with Ti addition, the spangle size decreased and the formability of GL improved [50].

With regard to corrosion mechanisms in cracking zone of deformed coating, two situations could be described: First, before penetration of cracks into the steel substrate, the corrosion mechanism should basically be consistent with that of non-deformed coating, exhibiting only fast corrosion expansion due to the occurred cracks. Second, after penetration of cracks into the steel substrate, the corresponding corrosion mechanism was consistent with the generally cut-edge corrosion mechanism. For wider cracks, corrosion cells were formed by the coating, with corrosive medium and steel substrate at both sides of the cracks [51, 52]. As the anode, the coating was corroded by oxidation (sacrificial anode). As the cathode, the reduction reaction occurred at the steel substrate, where it contributed to electron-transfer only but did not corrode (cathodic protection). At the crack central region, the steel substrate was not protected by the coating. Therefore, it formed a corrosion cell with corrosive medium, where it was rapidly corroded as the anode by oxidation. As cracks narrowed, the steel substrate within the cracking region was protected by the coating due to the sacrificial anode effect of the coating, and the electrochemical corrosion of steel substrate could be inhibited. Obviously, as spangle size increased, cracks in the coating after deformation widened, and the number of cracks penetrating the steel substrate increased. This reduced the cathodic protection effect and the permeation barrier effect of coating on corrosion medium, thus decreasing the corrosion resistance.

3.3 Effect of spangle size on paintability

The surface roughness (Ra) values of specimens with different spangle sizes before and after painting are shown in Figure 12. The Ra value of original (before painting) samples was estimated to 0.3-0.8 μm. Furthermore, Ra decreased with increasing spangle size. After painting of the specimens, the Ra reached around 0.1 μm. Figure 13 illustrates the 2-D profile curves of samples before and after painting measured with surface roughometer. Evident changes occurred on the surface profile curves,

where the surface became smoother after painting. This suggested that the paint filled depressions present on the original surface through self-flow-leveling effect, inducing smoother surfaces.

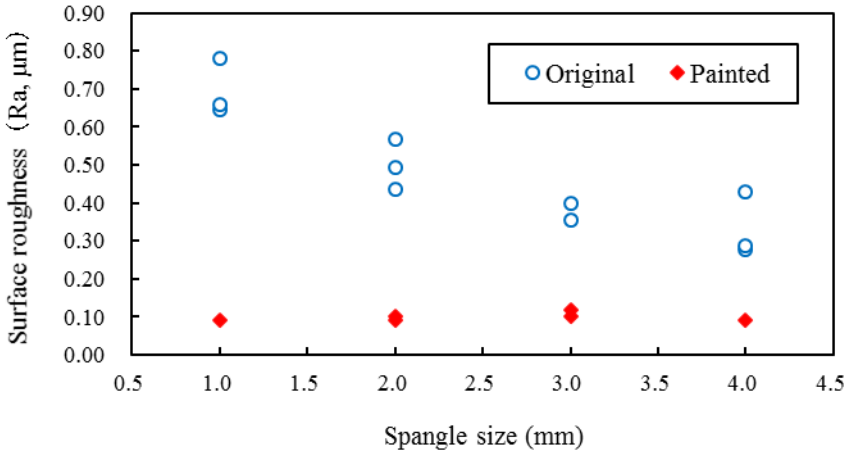

Figure 12. Surface roughness of specimens with different spangle sizes before and after painting.

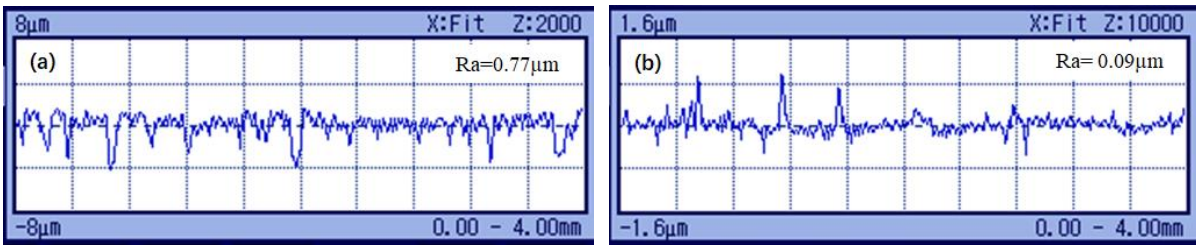

Figure 13. Examples of 2D profile curve of specimens for (a) original surface and (b) painted surface.

The gloss test results of the painted specimens are presented in Figure 14. The glossiness of specimens with different spangle sizes all ranged from 85-88, meeting user requirements. In addition, the cross-cut results of painted specimens indicated no occurrence of exfoliation in the painting layers of specimens with different spangle sizes (Figure 15), meaning 100% qualification.

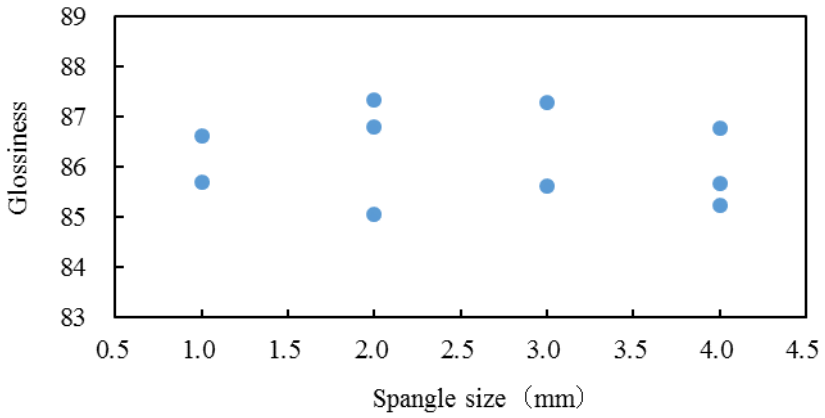

Figure 14. Surface gloss of painted specimens with different spangle sizes.

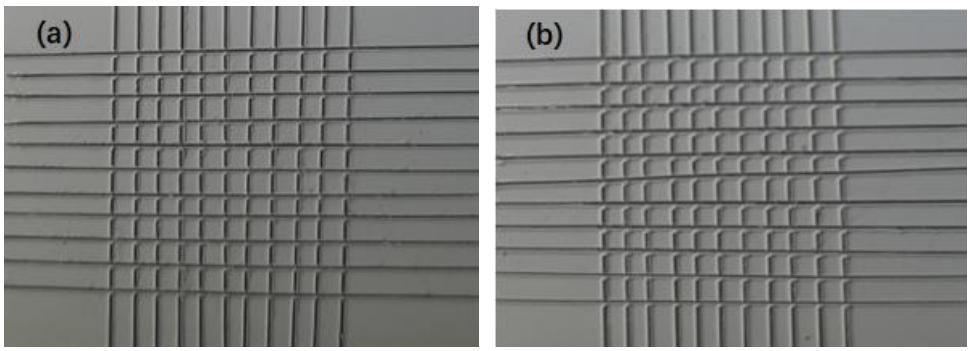

Figure 15. Resultant examples of adhesion test for painted specimens with (a) mini spangle and (b) large spangle.

In summary, no obvious differences in surface roughness, glossiness, or adhesion could be observed for painted specimens with different spangle sizes, demonstrating that spangle size had no obvious effect on specimen paintability.

The paintability of coated steel sheets are determined by their surface structures. The SEM analyses indicated that the spangle was normally composed of six sector regions (Figure 4). Al-rich dendrites and the Zn-rich phase between dendrites seemed uneven. According to 2-D profile curve measured by roughometer (Figure 13a), depressions were noticeable at the junction between two sector regions, with depths up to 4 μm. To confirm whether the inner region of the sectors was uneven, atomic force microscopy was used to analyze the surface micro-morphologies of three adjacent sector regions inside the spangle (Figure 16).

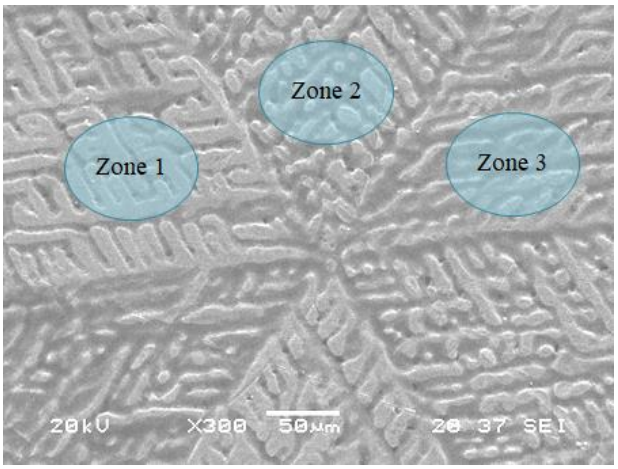

Figure 16. Diagram of atomic force microanalysis region.

The results confirmed that Al-rich dendrites and Zn-rich phase between dendrites within the sector region were indeed uneven. The depression depth reached up to 1 μm. The average roughness Ra of mini spangle was 53-101 nm, and that of large spangle was 5-32 nm (Figure 17). The hot-dip 55%Al-Zn alloy coating belonged to the dendrite structure and was generated by directional solidification, yielding uneven surface, which was similar with that of hot-dip pure Zn coating.

Previous studies [53, 54] showed that large spangle should have adverse effects on paintability of GI steel sheets, thus customers usually require mini spangle or non-spangle with skin-pass process. However, here, we showed that samples with large spangles also had good painting adhesion and appearance quality characteristics. These findings may be related to the painting method, where the results were only applicable to electrostatic powder spraying paint with large thickness and better smoothness features (self-flow-leveling performance).

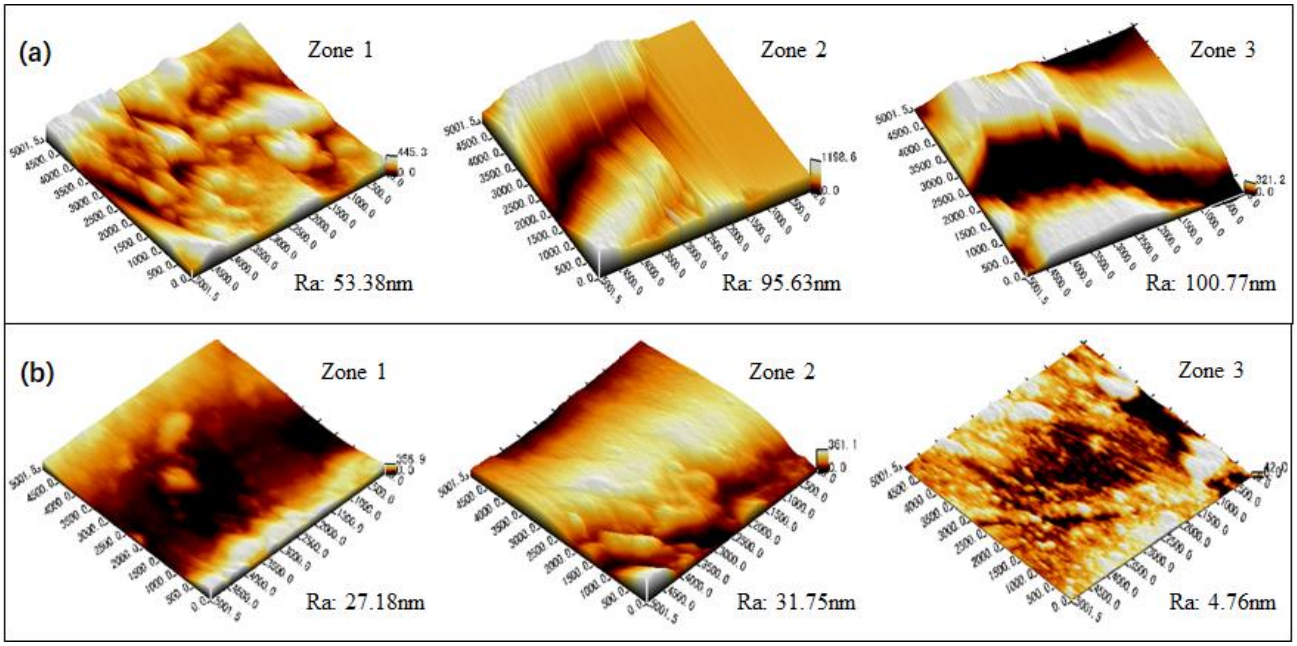

Figure 17. Atomic force micro-morphology of specimens with (a) mini spangle and (b) large spangle.

4. CONCLUSIONS

1) Different spangle sizes of GL coatings resulted in differences in Al-rich dendrite size, dendrite arm spacing, and surface unevenness. These showed adverse effects on corrosion resistance, formability, and paintability of the coating.

2) In a corrosive environment, corrosion occurred preferentially at the Zn-rich phase and expanded along the region between dendrites. As spangle size decreased, both Al-rich and Zn-rich phases refined, resulting in narrower and meandering corrosion expansion channels. The corrosion expansion was then easier to obstruct, thus improving the coating corrosion resistance.

3) During the deformation process, cracks originated from Zn-rich or Si-rich phase between dendrites, and expanded along the Zn-rich phase. As spangle size decreased, Al-rich and Zn-rich phases refined, and deformation coordination was promoted. Although the corresponding cracks after deformation were denser, their widths were smaller. Furthermore, the number of cracks penetrating into the steel substrate decreased, thus improving formability of coatings.

4) As spangle size increased, micro-surface roughness decreased while macro-unevenness increased, which was detrimental to painting adhesion and appearance quality. However, the current

experimental results showed no obvious relationship between spangle size and paintability. This may be due to the better self-flow-leveling performance of the electrostatic powder spraying paint and large thickness.

ACKNOWLEDGMENTS
The authors express their gratitude to Dr. Yongquan Qing from Northeastern University, Prof. Qianfeng Zhang from the Anhui University of Technology, and the experimental support from the Changhong Air conditioner Co.

References

1. J. D. Culcasi, C. I. Elsner and A. R. Di Sarli, *Mater. Res.*, 12 (2009) 273
2. S. K. Shukia, B. B. Saha, B. D. Triathi and R. Avtar, *J. Mater. Eng. Performance*, 19 (2010) 650
3. S. Chang and J. C. Shin, *Corros. Sci*., 36 (1994) 1425
4. H. Asgari, M. R. Toroghinejad and M. A. Golozar, *J. Mater. Process. Technol*., 198 (2008) 54
5. P. R. Sere, J. D. Culcasi, C. I. Elsner and A. R. Di Sarli, *Surf. Coat. Technol*., 122 (1999) 143
6. Y. Durandet, L. Strezov and N. Ebrill, Formation of Al-Zn-Si Coatings on Low Carbon Steel Substrates, Galvatech'98, Chiba, Japan, 1998, 20-23
7. R.Y. Chen and D. J. Willis, *Metall. Mater. Trans. A*, 36A (2005) 117
8. K. Tokuda, N. Shimoda and Y. Morimoto, A Study of Spangle Nucleation Process in 55%Al-Zn-1.6%Si Coatings, Galvatech'2011, Genova, Italy, 2011
9. D. Phelan, B. J. Xu and R. Dippenaar, *Mater. Sci. Eng. A*, 420 (2006) 144
10. B. J. Xu, D. Phelan, R. Dippenaar and D. Willis, Nucleation during Solidification of 55wt% Al-Zn-Si Alloy Coatings, Galvatech'04, Chicago, USA, 2004, 713-721.
11. A. Semoroz, Y. Durandet and M. Rappaz, *Acta Mater*., 49 (2001) 529
12. R. Y. Chen and D. Yuen, *Metall. Mater. Trans. A*, 43 (2012) 4711
13. J. H. Selverian, M. R. Notis and A. R. Marder, *J. Mater. Eng*., 9 (1987) 133
14. B.J. Xu, D. Phelan and R. Dippenaar, *Mater. Sci. Eng. A*, 473 (2008) 76
15. F. García, A. Salinas and E. Nava, *Mater. Letters*, 60 (72006) 75
16. G. X. Wu, J. Y. Zhang, Y. L. Ren and G. Y. Li, *Metall. Mater. Trans. A*, 43A (2012) 2011
17. X. F. Lai, H. P. Peng, J. H. Wang and C. J. Wu, *Surf. Eng*., 29 (2013) 390
18. E. Palma, J. M. Puente and M. Morcillo, *Corros. Sci*., 40 (1998) 61
19. P. R. Sere, M. Zapponi, C. I. Elsner and A. R. Di Sarli, *Corros. Sci.*, 40 (1998) 1711
20. A. R. Moreira, Z. Panossian, P.L. Camargo, M. F. Moreira and I. C. da Silva, *Corros. Sci*., 48 (2006) 564
21. X. Zhang, T. N. Vu, P. Volovitch, C. Leygraf, K. Ogle and I. O. Wallinder, *Appl. Surf. Sci*., 258 (2012) 4351
22. P. Qiu, C. Leygraf and I. O. Wallinder, *Mater. Chem. and Phys*., 133 (2012) 419
23. A. P. Yadav, A. Nishikata and T. Tsuru, *ISIJ Int*., 44 (2004) 1727
24. M. Granada, P. R. Sere, C. I. Elsner and A. R. Di Sarli, *MSAJ*, 12 (2015) 290
25. K. J. Fioravanti and H. W. Pickering, *Oxid. of Met*., 21 (1984) 285
26. T. A. Lowe, G. G. Wallace and A. K. Neufeld, *Corr. Sci*., 55 (2012) 180
27. I. O. Wallinder, W. He, P. E. Augustsson and C. Leygraf, *Corr. Sci*., 41 (1999) 2294
28. A. Humayun, Production & Performance of 55%Al-Zn Coated Sheet, Galvatech'95, Chicago, USA, 1995, 443-447
29. J. F. Willem, S. Claessens, H. Cormil, M. Fiorucci, A. Hennion and C. Xhoffer, Solidification Mechanisms of Aluzinc Coatings Effect on Spangle Size, Galvatech'01, Brussels, Belgium, 2001, 401–408
30. T. Ooi, CAMP-ISIJ, 8 (1995) 654

31. S.Hikino,T.Matsunaga, M.Aral, S. Bando and *La revue de Metall.*, 12 (1997) 168
32. J. H. Selverian, A. R. Marder and M. R. Notis, *Metall. Trans. A*, 19A (1988) 1193
33. H. Peng, G. Wu, W. Peng, B. Cao and J. Zhang, *Surf. Coat. Technol*., 327 (2017) 110
34. H. Peng, Q. Du, G. Wu, W. Dan, W. Hu and J. Zhang, *Surf. Coat. Technol*., 299 (2016) 56
35. R. Mathew, P. R. Stoddart, D. Nolan and Y. Durandet, *Surf. Coat. Technol*., 306 (2016) 490
36. W. Peng, G. Wu, X. Dai, J. Zhang, W. Hu and K. Chou, *TMS Light Metals*, (2015) 301
37. A. R. Marder. The Metallurgy of Zinc-Coated Steel [J]. *Prog. Mater. Sci*., 45 (2000) 193
38. X. Wang, J. Lu, C. Che and G. Kong, *Appl. Surf. Sci*., 254 (2008) 2466
39. S. Peng, J. Lu, C. Che, G. Kong and Q. Xu, *Appl. Surf. Sci*., 256 (2010) 5020
40. N. Pistofidis, G. Vourlias, S. Konidaris, E. Pavlidou and G. Stergioudis, *Mater. Lett.*, 61(2007) 2007
41. R. Parisot, S. Forest, A. Pineau, F. Grillon, X. Demonet and J. M. Mataigne, *Metall. Mater. Trans. A*, 35A (2004) 797
42. U. Ramamurty, S. Jana, Y. Kawamura and K. Chattopadhyay, *Acta Mater.*, 53(2005) 705
43. C. Zhang, F. Li and B. Wang, *J. Mater. Sci.*, 48 (2013) 4446
44. D. J. Willis and Z. F. Zhou, Factors Influencing the Ductility of 55% Al-Zn Coatings, Galvatech'95, Chicago, USA, 1995, 455-462
45. S. Graff, D. Steglich and W. Brocks, *Adv. Eng. Mater.*, 9 (2007) 803
46. R. Parisot, S. Forest, A. Pineau, F. Nguyen, X. Demonet and J. M. Mataigne, *Metall. Mater. Trans. A*, 35A (2004) 813
47. J. Zuo, L. Hou, J. Shi, H. Cui, L. Zhuang and J. Zhang, *Mater. Sci. Eng. A*, 702 (2017) 42
48. X. Wan, G. Li, B. Zhou and J. Ma, *J. Mater. Eng.*, 44 (2016) 29
49. S. J. Park, K. W. Jung, H. S. Koh, M. B. Moon and H. W. oh, Production of heavy gauged HY-Galvalume in Hyundai HYSCO, APGALVA 2009, Jeju, Korea, 2009
50. J. Xu, Q. Gu, Q. Li and H. Lu, *Metall. Mater. Trans. A*, 47A (2016) 6542
51. T. Iwa, T. Watase, Y. Hirano and K. Araga, On the Factors Generating the Red Rust in the Edge Faces of the Painted Steel Sheets for Outdoor Users, GALVATECH 2013 & APGALVA 2013, Beijing, China, 2013, 693–696
52. A.Nishikata, T. Tsuda and T. Tsuru, Production of heavy gauged HY-Galvalume in Hyundai HYSCO, APGALVA 2009, Jeju, Korea, 2009
53. M. Zapponi, A. Quiroga and T. Perez, *Surf. Coat. Technol*., 122 (1999) 18
54. P. Puomi, H. Fagerholm and J. Rosenholm, *J. Adhesion Sci. Technol*., 14 (2000) 583